

Freestanding LiPON: from Fundamental Study to Uniformly Dense Li Metal Deposition Under Zero External Pressure

Diyi Cheng¹, Thomas Wynn², Bingyu Lu², Bing Han², Ryosuke Shimizu², Bhagath Sreenarayanan², Maxwell Marple³, Yangyuchen Yang², Han Nguyen², Weikang Li², Guomin Zhu², Minghao Zhang^{2,*}, Ying Shirley Meng^{1,2,4*}

¹Materials Science and Engineering Program, University of California San Diego, La Jolla, CA 92121, USA

²Department of NanoEngineering, University of California San Diego, La Jolla, CA 92121, USA

³Physical and Life Science Directorate, Lawrence Livermore National Laboratory, Livermore, CA 94550, USA

⁴Pritzker School of Molecular Engineering, University of Chicago, Chicago, IL 60637, USA

*Corresponding Author E-mails: miz016@eng.ucsd.edu, shirleymeng@uchicago.edu

Abstract

Lithium phosphorus oxynitride (LiPON) is a well-known amorphous thin film solid electrolyte that has been extensively studied in the last three decades. Despite the promises to enable Li metal anode and various cathode materials, the presence of rigid substrate and LiPON's unique amorphous, air-sensitive characteristics set limitations to comprehensively understand its intrinsic properties for next-stage advancement and applications. This work demonstrates a different methodology to synthesize LiPON in a freestanding form that removes the substrate. The freestanding LiPON (FS-LiPON) exhibits remarkable flexibility, with controllable film thickness and large-scale production compatibility. Benefited from the freestanding form, solid-state nuclear magnetic resonance (ss-NMR) and differential scanning calorimetry (DSC) are able to attain high S/N ratio to determine the local bonding structures and glass transition temperature of LiPON. In the presence of interfacial stress and a seeding layer, FS-LiPON demonstrates a uniform and fully dense Li metal deposition without the aid of external pressure. Such a FS-LiPON film offers new opportunities for fundamental study of LiPON material and associated interfaces, and provide perspectives for interface engineering in bulk solid-state battery.

Introduction

Lithium phosphorus oxynitride (LiPON) is a thin film solid-state electrolyte (SSE) that is conventionally deposited on solid substrates. Substituting 5%-8% of O with N in Li_3PO_4 by radio-frequency (RF) sputtering, LiPON was first invented by Bates et al. in 1992.¹ LiPON rapidly drew research attention in the solid state battery field as it exhibits exemplary cyclability with a vast choices of electrode materials, i.e., LiCoO_2 ,² LiMn_2O_4 ,² $\text{LiNi}_{0.5}\text{Mn}_{1.5}\text{O}_4$,³ $\text{Li}_4\text{Ti}_5\text{O}_{12}$,⁴ and Li metal,²⁻⁴ etc. Over the three decades since the discovery of LiPON, numerous research efforts have been undertaken to shed light on the structure and properties of the material itself and associated interfaces, for the sake of gaining knowledge regarding the stable nature and performance of LiPON, and providing guidelines on engineering other SSEs for next generation lithium rechargeable batteries.

Interpretation of the intrinsic properties of LiPON, nevertheless, has been disputed due to the amorphous nature of LiPON, its air-sensitive characteristic, and the presence of solid substrate. One of the long-lasting debates pertains to the N bonding structure and its impact on the lithium transport properties in LiPON. Early studies on the chemistry of LiPON primarily relied on X-ray photoelectron spectroscopy (XPS), where two different N environments were identified and regarded as double-bridging N and triple-bridging N.⁵⁻⁷ Such peak assignment was in part due to the pervasive belief that the cross-linked configuration introduced by N incorporation is the key for the ionic conductivity enhancement of LiPON over Li_3PO_4 .⁷ Alternative ways that are suitable to probe local bonding environment such as neutron paired distribution function (PDF) and solid-state nuclear magnetic resonance (ss-NMR) were unable to validate this hypothesis in early time due to the difficulty to obtain enough signal-to-noise (S/N) ratio, as the presence of substrates beneath LiPON thin film largely limits the active material amount that can be filled into the spectrometer. Regardless, Lacivita et al. managed to obtain enough sample for neutron PDF measurements by scrapping LiPON from the substrate and ruled out the existence of triple-bridging N, instead double-bridging N and apical N are the prevalent forms of N environments in LiPON.^{8,9}

Aside from the LiPON bulk structure, the interface stability between electrode materials and LiPON were also studied. Despite the knowledge on cathode-associated interfaces in early work¹⁰⁻¹² and recent insights gained on Li metal/LiPON interface via the advances of cryogenic electron microscopy,^{13,14} the electro-chemo-mechanical properties of SSE/electrode interfaces are also regarded as critical metrics to determine the mechanical behavior at the interface during cycling, which can alter the stability and the cycle life of solid-state batteries.¹⁵ However, there

has been a lack of literature studying the mechanical properties of LiPON. Herbert et al. measured the Young's modulus of LiPON by nanoindentation and obtained a value of 77 GPa.¹⁶ A similar Young's modulus was documented by Xu et al. using picosecond ultrasonics measurement.¹⁷ Such high modulus is proposed to give LiPON a rigid characteristic that accounts for its ability to suppress Li dendrite protrusion during cycling and contribute to its remarkable cyclability. Nevertheless, the long-term air exposure of LiPON during nanoindentation measurements and many approximations made during picosecond ultrasonics data analysis have weakened the conclusions. The fact that there is limited mechanical study on LiPON is, inevitably, also attributed to the presence of solid substrates, otherwise a wider selection of mechanical characterizations such as bending and stretching tests, etc. can be utilized for examination.

Such dilemma associated with the substrate and insufficient active material amount for measurements originates from the conventional synthesis methods of LiPON thin film. In fact, a variety of existing methods are available to synthesize LiPON, including RF sputtering,¹ pulsed laser deposition (PLD),⁶ atomic layer deposition (ALD),¹⁸ ammonolysis, inductively coupled plasma (ICP) and ball milling, etc. Despite the diverse compositions of the LiPON variants yielded by different methods (**Supplementary Table S1**), most of these processes require the use of a solid substrate (i.e., silicon, glass, alumina, or sapphire, etc.) for LiPON to be deposited on, especially for vacuum deposition techniques. Those methods getting around the use of substrate such as ammonolysis, ICP or ball milling suffer either from the altered LiPON properties or increased interfacial impedance within LiPON powders.^{19–21} For the sake of enabling further fundamental characterizations, the removal of the substrate during LiPON synthesis will serve as a sound solution. On another note, removing the substrate is also promising to largely improve the energy density of thin film solid-state battery, as the substrate usually weighs several to hundreds of times more than the active materials.

Inspired by the semiconductor industry, where photoresist is commonly used as a mask material that can withstand plasma-assisted deposition and easy to remove using organic solvents, herein we introduce a different methodology to synthesize a LiPON thin film that is in freestanding form without a rigid solid substrate. The as-obtained freestanding LiPON (FS-LiPON) thin film exhibits transparency and a remarkable flexibility. The proposed methodology is validated to barely alter the LiPON structure, chemical bonding environments, and electronic properties by subsequent characterizations, compared with the substrate-based analogues in literature. Differential scanning calorimetry (DSC) and ss-NMR are able to obtain enhanced S/N ratio using FS-LiPON, illustrating the advantage and potential of FS-LiPON for

fundamental studies. With the aid of interfacial stress between at Cu/FS-LiPON and the presence of an Au seeding layer, we further demonstrate a uniform and fully dense Li metal electrochemical deposition under zero external pressure. The proposed principles and solutions for enabling uniform Li metal deposition provide new insights on interface engineering in bulk Li metal solid-state batteries.

Results and Discussion

A Flexible Freestanding LiPON Thin Film

Figure 1A depicts the fabrication procedure of FS-LiPON. Before employing RF sputtering, a spin-coating method was used to coat clean glass substrate with photoresist. Details about the spin coating recipe can be found in the experimental procedure section. LiPON thin film was then deposited onto the coated glass substrate by RF sputtering under N₂ plasma. After RF sputtering, LiPON sample was transferred into a container filled with Dimethyl carbonate (DMC) solvent in an argon-filled glove box. The substrate and LiPON film were fully immersed in DMC for overnight. Photoresist was then dissolved by DMC, after which LiPON film delaminated from the glass substrate and ready for pickup. Unlike the common way of producing LiPON thin film on a solid substrate, this method yields LiPON film in a freestanding form and exhibits transparency and remarkable flexibility as shown in **Figure 1B** and **Supplementary Video S1**. Such characteristics indicate LiPON being a soft material, in stark contrast with previous observations in literature.^{16,17} Depending on the substrate size, deposition area and deposition time, the area, thickness and sample amount of FS-LiPON can be controlled following this procedure (**Supplementary Figure 1**).

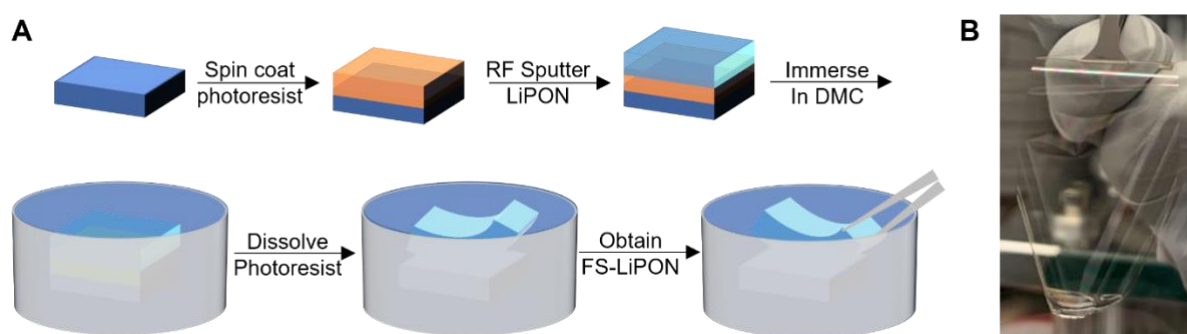


Figure 1. (A) Schematic of synthesis procedure for FS-LiPON. (B) Optical photo of a transparent and flexible FS-LiPON thin film.

To validate that the structure, chemical bonding environments and electrical properties of FS-LiPON are not affected during the above synthesis procedure, a variety of characterizations were carried out. The cross-section morphology and corresponding energy-dispersive X-ray spectroscopy (EDS) elemental mapping were first examined and shown in **Supplementary Figure S2**. The fully dense feature of LiPON is retained in this 3.7- μm -thick film and P, O, and

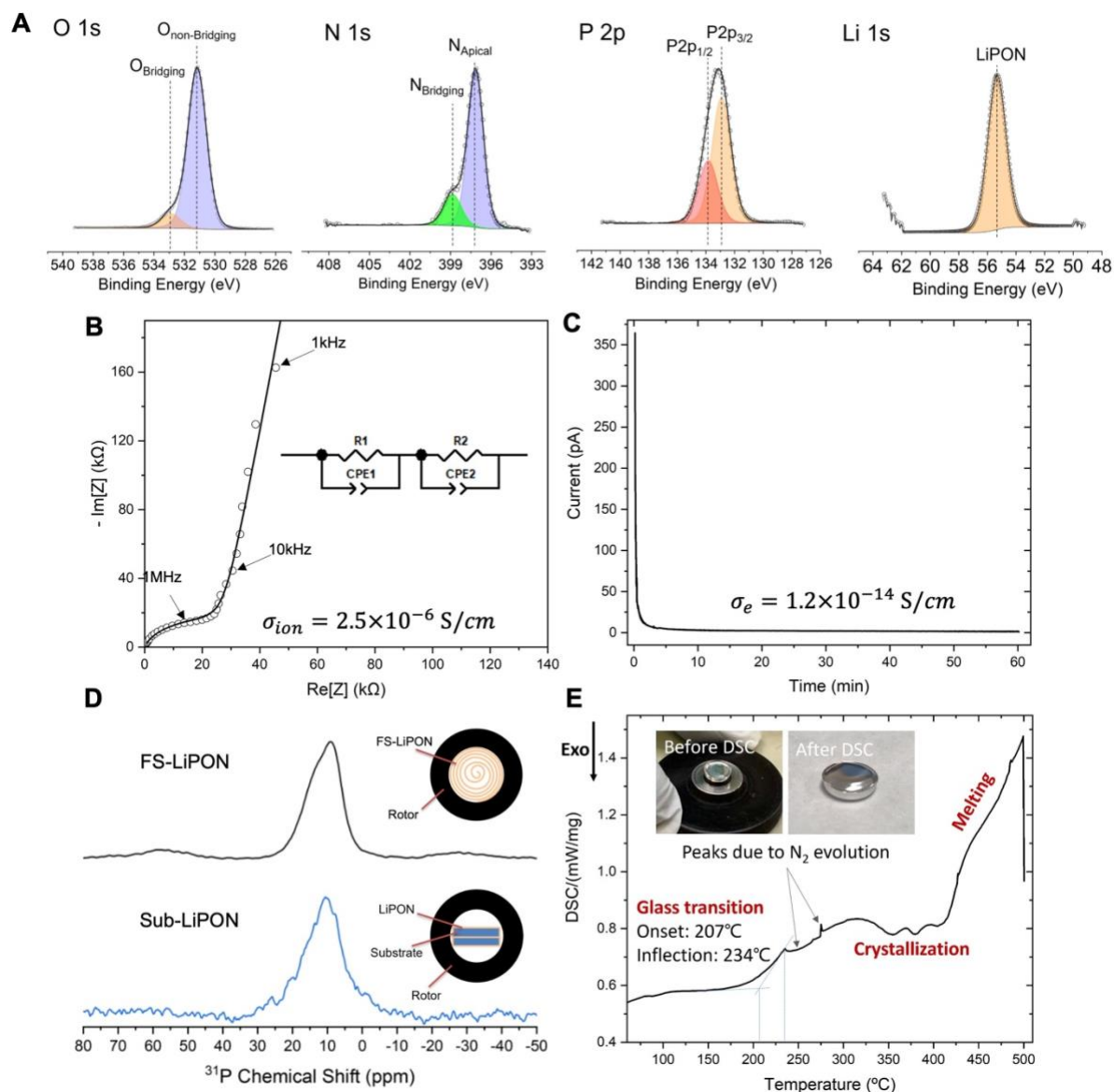


Figure 2. Chemical bonding environments, electrical and thermal properties of FS-LiPON. (A) XPS spectra of O 1s, N 1s, P 2p and Li 1s regions of FS-LiPON thin film. (B) EIS plot and (C) DC polarization plot of FS-LiPON. (D) ^{31}P NMR results of FS-LiPON and Sub-LiPON, with corresponding schematic cross-section of the ss-NMR rotor. (E) DSC analysis of FS-LiPON

N elements are uniformly distributed across the sample. **Supplementary Figure S3A** shows the X-ray diffraction (XRD) results of FS-LiPON, where no diffraction spot is present in the

top diagram, and the integrated signal at the bottom only exhibits an amorphous feature around 23 degrees in 2θ , indicating the amorphous characteristic of FS-LiPON. **Figure 2A** displays the XPS result of FS-LiPON thin film, where O 1s, N 1s, P 2p and Li 1s regions manifest consistent features with substrate-based LiPON (Sub-LiPON) that are included in **Supplementary Figure S4** and in literature,^{7,22} demonstrating that the chemical bonding environments are retained in the freestanding film. Moreover, the elemental mapping results by EDS on FS-LiPON surface in **Supplementary Figure S3B** confirm that N, P and O elements are uniformly distributed on the surface of the FS-LiPON film. Serving as an SSE, Sub-LiPON is an ionic conductor whilst an excellent electrical insulator. Electrochemical impedance spectroscopy (EIS) and direct-current (DC) polarization were subsequently employed to examine the electrical properties of FS-LiPON. The EIS spectrum in **Figure 2B** yields an ionic conductivity of 2.5×10^{-6} S/cm for FS-LiPON, better than the LiPON analogues produced by PLD and ALD methods.^{6,18} DC polarization plot in **Figure 2C** gives an electronic conductivity of 1.2×10^{-14} S/cm, on the order of Sub-LiPON as reported in literature.^{7,23} Based on above results, FS-LiPON exhibits consistent properties with Sub-LiPON regardless of its freestanding form.

New Opportunities for Fundamental Study of LiPON

As a model example to demonstrate the advantage of applying FS-LiPON for spectroscopic characterization, ss-NMR was performed on FS-LiPON and the results are shown in **Figure 2D**. FS-LiPON illustrates a similar ^{31}P chemical shift compared to Sub-LiPON, agreeing with the XPS evidence. Notably, the NMR spectra acquired on FS-LiPON gains a much higher S/N ratio than Sub-LiPON due to the absence of solid substrate and thus an increased active material amount. The well-distinguishable ss-NMR results enabled a more comprehensive understanding on the local bonding structure of LiPON in our recent work, where ss-NMR coupled with density functional theory calculations have identified the majority of structural units to be PO_4 tetrahedra with nitrogen occupation of bridging and apical sites.⁹ Such knowledge cannot be obtained using Sub-LiPON, as the S/N ratio is too low to perform descent peak fitting and quantification.

Another advantage of FS-LiPON as for fundamental study ties in its thermal property analysis. LiPON is known to be a glass material for which the glass transition temperature is one of the most important metrics to determine its metastable states and application environments. Nevertheless, due to the limitation of active material for measurement,

previously documented trials using DSC to examine the glass transition temperature of Sub-LiPON failed to capture clear transition behaviors.²⁴ In this regard, DSC was conducted on FS-LiPON and results are plotted in **Figure 2E**, where an obvious glass transition was observed with an onset temperature of 207 °C and inflection around 234 °C, consistent with LiPON glass transition temperature studied using spectroscopic ellipsometry.²⁵ Subsequent thermal response in **Figure 2E** further captured the crystallization and melting processes of LiPON, with gas release observed during heating.

Outlooking the potential of FS-LiPON in the fundamental research, more chances are opened up to investigate the intrinsic properties of LiPON, such as its “soft” characteristic by mechanical tests. Preliminary results of FS-LiPON film stiffening after 3-day air exposure are demonstrated in **Supplementary Figure S5** and **Supplementary Video S2**, stressing on the importance of inert environment protection during the mechanical examination, which could eventually yield a more comprehensive picture of the stability of LiPON against various electrodes materials.

Electrochemical Activity of FS-LiPON

Apart from the intrinsic property aspect, FS-LiPON is also demonstrated to be applicable in electrochemical devices. A FS-LiPON Li-Cu cell was fabricated using the configuration shown in **Figure 3A**, where Cu and Li electrodes with the same designed area were aligned across FS-LiPON film. As-fabricated Li-Cu cell harnesses the flexible nature of FS-LiPON as shown in **Figure 3B**. The flexibility of the cell was further demonstrated in **Figure 3C**, where the cell was bent by the tweezer while still able to sustain Li metal plating and stripping capability afterwards. **Figure 3D** shows the voltage curve of the Li-Cu cell during constant-current measurement. When a current of -50 nA is applied, the cell exhibits a voltage dip and reaches an overpotential of ~-1V, after which a stable plating process proceeds. When altering the current direction, a stripping curve feature is obtained. The cell demonstrated a stable plating and stripping over 13 cycles without short-circuiting, indicating the ability of FS-LiPON to shuttle lithium ions. The relatively high overpotential is likely due to the large thickness of FS-LiPON film, which could be reduced through future engineering efforts. It's noteworthy that owing to the unique configuration of FS-LiPON Li-Cu cell, no external pressure was applied to the cycled cell.

The plated Li metal morphology in FS-LiPON system was then examined by cryogenic focused ion beam/scanning electron microscopy (cryo-FIB/SEM). **Figure 3E** displays the cross-section morphology of pristine Li-Cu cell, where no extra layer is observed between Cu

and FS-LiPON before plating and the evaporated Li metal on the other side of FS-LiPON appears fully dense. Note that cryogenic protection during FIB milling is crucial to preserve the pristine morphology and chemistry of Li metal, as reported elsewhere before²⁶ and demonstrated in **Supplementary Figure S6**. After a constant current plating, Li-Cu cell shows a dense Li layer with dark contrast between Cu and FS-LiPON in **Figure 3F**. Associated Li-Cu cell voltage curve is plotted in **Supplementary Figure S7**. EDS mapping on a plated Li-Cu cell in **Supplementary Figure S8** illustrates the presence of Cu, P, O and Ga over corresponding regions. Due to the inability of regular EDS detectors to distinguish Li signal,

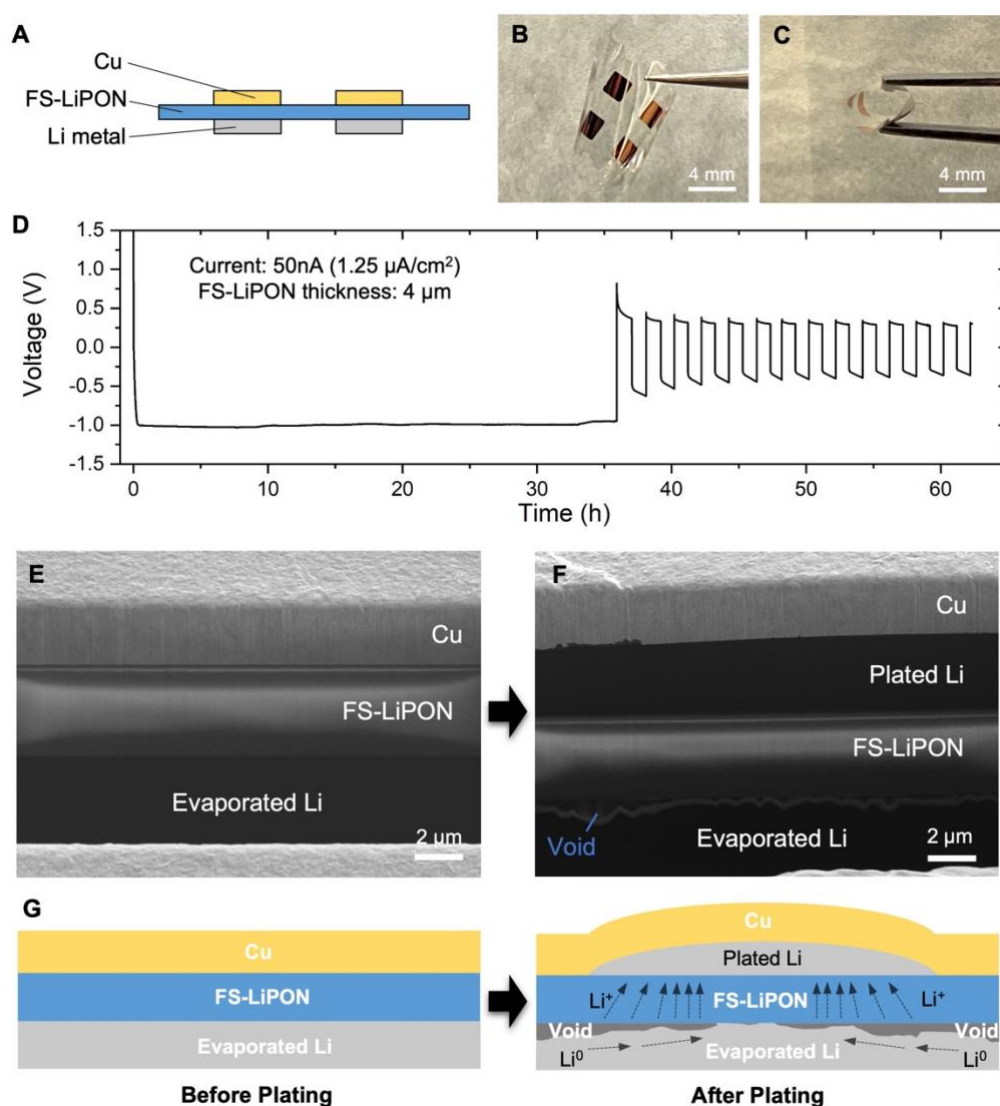


Figure 3. (A) Cross-section schematic of the FS-LiPON Li-Cu cell. Photos of FS-LiPON Li-Cu cell from top view (B) and upon bending (C). (D) Voltage curve of Li metal plating and stripping in a FS-LiPON Li-Cu cell. Cross-section cryo-FIB/SEM images of Li-Cu cell before Li metal plating (E) and after Li metal plating (F). (G) Schematic showing the proposed non-uniform void formation mechanism during Li metal plating.

the absence of EDS signal in the dense layers between Cu and FS-LiPON, and in the evaporated Li metal region suggests the existence of plated Li metal above FS-LiPON. Such features indicate a fully dense Li metal electrochemical deposition was realized by this FS-LiPON configuration when no external pressure was present.

Intriguingly, in **Supplementary Figure S8** a void region was observed between FS-LiPON and evaporated Li metal, as hinted by the aggregation of Ga signal that is commonly caused by redeposition during FIB milling and that is prevalently found at the bottom of void region after FIB milling.¹³ A similar void feature is also observed in **Figure 3F**, where a gap presents between FS-LiPON and evaporated Li. Though the theoretical thickness of plated Li metal is calculated to be 1 μm based on the areal capacity, the observing region shows a plated Li metal thickness around 4 μm in **Figure 3F**. Top-view SEM image in **Supplementary Figure S9** displays various bumps distributed over the Cu surface after plating. **Figure 3G** delineates the plating process occurring in Li-Cu cell without pressure control. Before plating, each constituent in the cell is distinguishable by the well-defined interfaces. After plating, plated Li metal forces up the Cu layer around the initial nucleation site, while the non-uniform lithium-ion flux within FS-LiPON drives lithium atoms around the vicinity of the nucleation site to migrate and compensate the metallic lithium reservoir right under the nucleation site. Therefore, void regions are formed around the nucleation site after plating is completed. Above results suggest that Li metal plating is non-uniform across the FS-LiPON when cycling without external pressure. However, wherever it is plated between Cu and FS-LiPON, Li metal remains fully dense.

From a side view, the electrochemical deposition of Li metal in liquid electrolyte has long been problematic due to the uncontrollable mass transfer, non-uniform nucleation, and continuous growth of solid electrolyte interphase (SEI), which render the deposited Li metal torturous and whisker-like.^{27,28} The electrochemically deposited Li metal in other SSE systems (i.e. $\text{Li}_7\text{La}_3\text{Zr}_2\text{O}_{12}$ and $\text{Li}_6\text{PS}_5\text{Cl}$, etc.), however, appears fully dense regardless of dendrite formation issues. Such morphological differences are likely due to the presence of external pressure on the order of several MPa in SSE system.^{29,30} Note that with external pressure control, recently Fang et al. managed to obtain nearly fully dense Li metal deposition in liquid electrolyte system when the cell runs under an optimized pressure of 350 kPa.²⁸

Enabling Fully Dense, Uniform Li Deposition Without External Pressure

Analogous to the cases of other solid electrolyte systems, fully dense Li metal plating has

also been demonstrated in FS-LiPON system. Nevertheless, it is noteworthy that there is no external pressure applied on the LiPON system when the fully dense feature of plated Li is obtained, suggesting the possible presence of interfacial stress that could act as internal pressure to promote Li metal yielding and facilitate subsequent dense Li metal deposition. Previous work by Motoyama et al. proposed a model to simulate the interfacial stress between Li metal and Cu current collector after plating, where they used an imaginary Li metal sphere and estimated the radial stress on Li metal surface based on Hoop stress formula.³¹

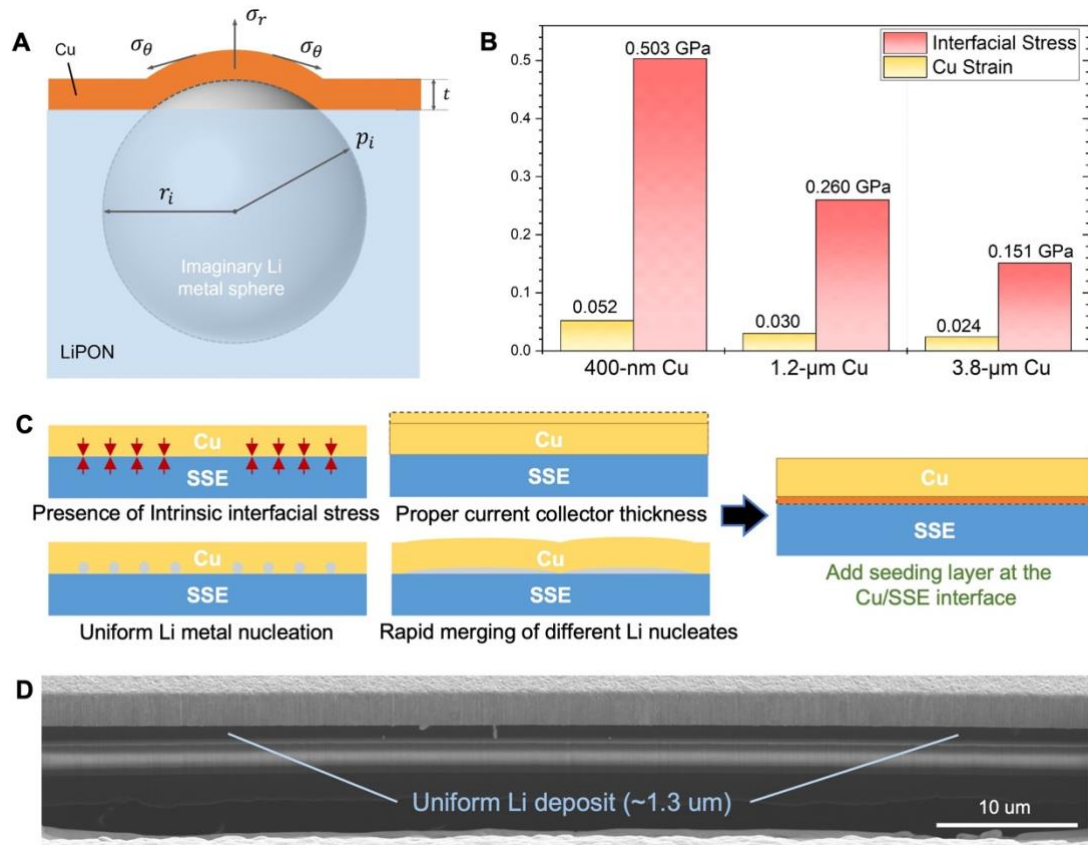


Figure 4. (A) Schematic of the interface model for interfacial stress simulation, where P_i is the interfacial stress between Li and Cu, σ_θ is the stress on Cu in the circumferential directions, σ_r is the stress on Cu in the radial direction, t is the thickness of Cu, r_i is the radius of Li metal imaginary sphere. (B) Cu strain and simulated interfacial stress in Li-Cu cell with regard to different Cu thicknesses. (C) Proposed principles and solution to achieve uniform Li metal deposition in solid system. (D) Cryo-FIB/SEM image showing uniform Li deposition realized by adding Au seeding layer in FS-LiPON Li-Cu cell.

Employing the similar stress analysis model shown in **Figure 4A**, we obtained the formula as follows:

$$P_i = \frac{\varepsilon_{Cu} E_{Cu}}{(1 - \nu_{Cu})} \cdot \left\{ \frac{3(r_i + t)^3}{2[(r_i + t)^3 - r_i^3]} - \frac{\nu_{Cu}}{1 - \nu_{Cu}} \right\}^{-1}$$

where P_i is the interfacial stress between Li and Cu, ε_{Cu} is strain in the circumferential directions, E_{Cu} is Young's modulus of Cu, t is the thickness of Cu, r_i is the radius of Li metal imaginary sphere, κ is the curvature of Cu, ν_{Cu} is the Poisson's ratio of Cu. The input values of above parameters were extracted from **Supplementary Figure S10** and listed in **Supplementary Figure S11**. **Figure 4B** shows the Cu strain and resulting interfacial stresses in the Li-Cu cells with different Cu thickness, ranging from 0.151 GPa to 0.503 GPa as Cu strain ramps from 0.024 to 0.052. Obtained stresses herein are hundreds of times higher than the external pressure applied on bulk SSE analogues. Such high interfacial stress present at Cu/Li interface confines Li metal morphology to achieve fully dense feature. Based on aforementioned stress formula, interfacial stress is inversely proportional to the Li deposit diameter and proportional to Cu strain, suggesting that Li metal deposit tends to have plenary growth so that overall stress can be released, resulting in more uniform coverage of Li metal on LiPON and less chance of dendrite formation. As such, we propose several criteria that need to be considered while building ideal configuration for Li metal plating in solid state system. As shown in **Figure 4C**, intrinsic interfacial stress is essential to generate pressure during Li metal plating without the aid of external pressure; proper current collector thickness is needed to confine Li metal morphology while maintaining its own structural integrity; uniform Li metal nucleation and rapid merging of different Li nucleates helps reduce the plastic deformation of current collector to prolong the cyclability. Consequently, one solution to achieve uniform Li metal deposition is adding seeding layer at Cu/SSE interface, as to facilitate uniform Li metal nucleation and subsequent uniform and dense Li metal growth. In this case, Au seeding layer was selected to demonstrate the hypothesis, since metal elements that alloy with Li metal tend to be lithiophilic and can regulate nucleation behavior.³² Prior to depositing Cu on FS-LiPON, a 3-nm-thick Au layer was first evaporated on FS-LiPON. Surface SEM image and EDS results in **Supplementary Figure S12** validates the Au film formed on FS-LiPON before Li-Cu cell fabrication. After electrochemical plating with zero external pressure (**Supplementary Figure S13A**), Cu surface remains relatively smooth as shown in **Supplementary Figure S13B**, suggesting a uniform Li metal deposition beneath. **Figure 4D** shows the cross-section image of the Li-Cu cell with Au seeding layer after plating. Measured thickness of Li metal deposit is $\sim 1.3 \mu\text{m}$, close to the thickness calculated from areal capacity (**Supplementary Figure S13A**). Li metal deposit appears not only full dense, but also uniform

across the whole region. Small inclusions found in plated Li metal layer are likely the Li-Au alloy based on cross-section EDS in **Supplementary Figure S14**. Based on above results, with the aid of interfacial stress and seeding layer, uniform and fully dense Li metal deposition can be realized in solid-state system under zero external pressure, which serves as a tribute to the exploration of interface engineering in bulk solid-state batteries.

Conclusion and Outlook

This work presents a different methodology to produce a thin film SSE in a freestanding form that manifests transparency and remarkable flexibility. Basic characterizations validated the chemical compatibility of FS-LiPON against materials used during synthesis procedure. The absence of substrate for FS-LiPON is leveraged in fundamental study, as illustrated by a largely improve S/N ratio in ss-NMR and DSC measurements. A further demonstration of an electrochemical cell employing FS-LiPON shows its ability to conduct lithium ions. Stress analysis at Li/Cu interface suggests the presence of a high compressive stress in the order of 10^{-1} GPa, which facilitates Li metal yielding and is the key for a dendrite-free, dense Li metal morphology. With the further aid of Au seeding layer, a fully dense and uniform Li metal deposition was realized under zero external pressure. The ideal conditions proposed for uniform Li metal deposition and the practice combining interfacial stress and seeding layer provide new perspectives for interface engineering. With the freestanding form of LiPON thin films, opportunities have been opened up for a wider application of LiPON material. When coupled with casted cathodes, FS-LiPON can potentially be utilized as the SSE and enable Li metal solid-state batteries without external pressure, which is otherwise an extra metric that awaits solution for practical use.

Experimental Procedures

Photoresist Spin Coating

AZ1512 photoresist (from EMD Performance Materials Corp.) is coated on clean glass substrate by spin coating. The heater temperature for prebake and postbake was set as 100°C. The spinning recipe includes 500 RPM for 20s, 1000 RPM for 20s and 2000 RPM for 60s. The resulting photoresist layer thickness is about 1.7 μm .

Thin Film Deposition

LiPON thin film was deposited on photoresist-coated glass substrate by RF sputtering using a crystalline Li_3PO_4 target (2" in diameter, from Plasmaterials, Inc.) in UHP nitrogen atmosphere. The base pressure of the sputtering system was 3.0×10^{-6} Torr. LiPON deposition used a power of 50W and nitrogen gas pressure of 15 mTorr. The as-deposited LiPON thin film was 3.7 μm in thickness with a growth rate of ~ 0.46 $\text{\AA}/\text{min}$. The copper pads for EIS tests and current collector were deposited by thermal evaporation using copper pellets (from Kurt J. Lesker, 99.99% purity). Growth rate is 1 $\text{\AA}/\text{s}$. Li metal anode for the Li-Cu cell was deposited by thermal evaporation with a base pressure of 2.5×10^{-8} Torr and growth rate of 3-4 $\text{\AA}/\text{s}$. The Au seeding layer was deposited by thermal evaporation using gold pellets (from Kurt J. Lesker, 99.99% purity). Growth rate is 1.5 $\text{\AA}/\text{s}$.

X-Ray Diffraction

The powder crystal X-ray diffraction was carried out on a Bruker micro focused rotating anode, with double bounced focusing optics resulting in Cu $\text{K}_{\alpha 1}$ and $\text{K}_{\alpha 2}$ radiation ($\lambda_{\text{avg}} = 1.54178$ \AA) focused on the sample. A sample of FS-LiPON was mounted onto a four circle Kappa geometry goniometer with APEX II CCD detector.

Microscopic Morphology and Chemical Analysis

Scanning Electron Microscopy (SEM) was performed using an FEI Apreo SEM with an electron beam energy of 5 keV and an electron beam current of 0.1 nA. The energy dispersive spectroscopy X-Ray spectroscopy (EDS) was collected using an electron beam energy of 5 keV by the Pathfinder EDS software from Thermo Scientific.

X-ray Photoelectron Spectroscopy

X-Ray photoelectron spectroscopy (XPS) was performed in an AXIS Supra XPS by Kratos Analytical. XPS spectra were collected using a monochromatized Al K α radiation ($h\nu = 1486.7$ eV) under a base pressure of 10^{-9} Torr. To avoid moisture and air exposure, a nitrogen filled glovebox was directly connected to XPS spectrometer. All XPS measurements were collected with a $300 \times 700 \mu\text{m}^2$ spot size. Survey scans were performed with a step size of 1.0 eV, followed by a high-resolution scan with 0.1 eV resolution, for lithium 1s, carbon 1s, oxygen 1s, nitrogen 1s, and phosphorous 2p regions. A 5 keV Ar plasma etching source was used for surface etching with a pre-etching for 5 s, etching for 60 s and post-etching for 10 s. All spectra were calibrated with adventitious carbon 1s (284.6 eV) and analyzed by CasaXPS software.

Electrochemical Measurements

A Biologic SP-200 potentiostat was used to measure the electrochemical impedance spectroscopy (EIS) and DC polarization of FS-LiPON. The frequency range for EIS was 3 MHz to 100 mHz with an amplitude of 10 mV and the obtained data fitted with a linear least square fitting method. The constant voltage used for DC polarization is 1V.

Solid-state Nuclear Magnetic Resonance

The NMR measurements performed on Sub-LiPON and FS-LiPON were collected using a 4 mm X/H channel Revolution probe on a 400 MHz (9.4 T) Bruker Biospin Avance Neo, operating at 161.97 MHz for ^{31}P . The samples were packed within a 4 mm pencil-type ZrO_2 rotor and spun at 10 kHz. The ^{31}P spectra were collected as a rotor synchronized Hahn echo experiment with a 90° pulse of 2.4 μs (B_1 field strength ~ 104 kHz). Hahn echo experiments were processed from the top of the echo to remove the effects of ring down from the FID. The recycle delays used for the 1D experiments was 25 s.

Differential Scanning Calorimetry

The Differential Scanning Calorimetry (DSC) measurement was conducted with DSC 214 Polyma (Netzsch). The temperature range was from 50°C to 500°C with a heating rate of $10^\circ\text{C}/\text{min}$. The DSC measurement was conducted under N_2 environment. All samples were sealed in aluminum pans in an Argon-filled glovebox to reduce contamination.

Cryogenic Focused Ion Beam/Scanning Electron Microscopy

A FEI Scios DualBeam FIB/SEM equipped with cryo-stage was used to observe the surface and cross-section morphology of plated Li metal in FS-LiPON Li-Cu cell. The operating voltage of electron beam was 5 kV. Emission current of electron beam was set to 25 pA to minimize potential damage of electron beam. A gallium ion beam source was used to mill and thin the sample. The operating voltage of ion beam source was 30 kV. Emission currents of ion beam were chosen for different purposes, i.e., 10 pA for imaging by ion beam, 0.1 nA for cross-section cleaning and 3 nA for pattern milling. To preserve the Li metal pristine morphology, a cryo-stage was used during pattern milling and cross-section cleaning processes, where the temperature of cryo-stage was maintained at around -185°C due to heat exchanging with cooled nitrogen gas.

Acknowledgements

The authors gratefully acknowledge funding support from the U.S. Department of Energy, Office of Basic Energy Sciences, under Award Number DE-SC0002357. FIB/SEM This work was performed in part at the San Diego Nanotechnology Infrastructure (SDNI) of UCSD, a member of the National Nanotechnology Coordinated Infrastructure, which is supported by the National Science Foundation (Grant ECCS-2025752). NMR was performed under the auspices of the US Department of Energy by LLNL under contract number DE-AC52-07NA27344. XPS and DSC were performed at the UC Irvine Materials Research Institute (IMRI) using instrumentation funded in part by the National Science Foundation Major Research Instrumentation Program under grant no. CHE-1338173 and DMR-2011967.

Author Contributions

D.C., M.Z. and Y.S.M conceived the ideas. D.C., T.W., B.L., R.S. and B.S. prepared the thin film sample. The FS-LiPON Li-Cu cell was designed by D.C. B.H., M.Z. and G.Z., and fabricated by D.C. M.M. performed and analyzed ss-NMR measurements. D.C. conducted cryo-FIB/SEM and electrical measurements. D.C. and H.N. collected XRD data. D.C., Y.Y. and W.L. collected XPS data. D.C., M.Z., Y.S.M., T.W., G.Z. and B.H. co-wrote the manuscript. All authors discussed the results and commented on the manuscript. All authors have approved the final manuscript.

Declaration of Interests

The authors declare no competing interests.

References

1. J.B. Bates, N.J. Dudney, G.R. Gruzalski, R.A. Zuhr, A. Choudhury, C. F. L. Electrical properties of amorphous lithium electrolyte thin films. *Solid State Ionics* **29**, 42–44 (1992).
2. Dudney, N. J. Solid-state thin-film rechargeable batteries. *Mater. Sci. Eng. B Solid-State Mater. Adv. Technol.* **116**, 245–249 (2005).
3. Li, J., Ma, C., Chi, M., Liang, C. & Dudney, N. J. Solid electrolyte: The key for high-voltage lithium batteries. *Adv. Energy Mater.* **5**, 1–6 (2015).
4. Put, B. *et al.* Plasma-Assisted ALD of LiPO(N) for Solid State Batteries. *J. Electrochem. Soc.* **166**, A1239–A1242 (2019).
5. Nimisha, C. S., Rao, G. M., Munichandraiah, N., Natarajan, G. & Cameron, D. C. Chemical and microstructural modifications in LiPON thin films exposed to atmospheric humidity. *Solid State Ionics* **185**, 47–51 (2011).
6. Zhao, S., Fu, Z. & Qin, Q. A solid-state electrolyte lithium phosphorus oxynitride film prepared by pulsed laser deposition. *Thin Solid Films* **415**, 108–113 (2002).
7. Bates, J. B. *et al.* Fabrication and characterization of amorphous lithium electrolyte thin films and rechargeable thin-film batteries. *J. Power Sources* **43**, 103–110 (1993).
8. Lacivita, V. *et al.* Resolving the Amorphous Structure of Lithium Phosphorus Oxynitride (Lipon). *J. Am. Chem. Soc.* **140**, 11029–11038 (2018).
9. Marple, M. A. T. *et al.* Local Structure of Glassy Lithium Phosphorus Oxynitride Thin Films: A Combined Experimental and Ab Initio Approach. *Angew. Chemie - Int. Ed.* **59**, 22185–22193 (2020).
10. Santhanagopalan, D. *et al.* Interface limited lithium transport in solid-state batteries. *J. Phys. Chem. Lett.* **5**, 298–303 (2014).
11. Wang, Z. *et al.* In situ STEM-EELS observation of nanoscale interfacial phenomena in all-solid-state batteries. *Nano Lett.* **16**, 3760–3767 (2016).
12. Wang, Z. *et al.* Effects of cathode electrolyte interfacial (CEI) layer on long term cycling of all-solid-state thin-film batteries. *J. Power Sources* **324**, 342–348 (2016).
13. Cheng, D. *et al.* Unveiling the Stable Nature of the Solid Electrolyte Interphase between Lithium Metal and Lipon Via Cryogenic Electron Microscopy. *Joule* **4**, 2484–2500 (2020).
14. Hood, Z. D. *et al.* Elucidating Interfacial Stability between Lithium Metal Anode and Li Phosphorus Oxynitride via in Situ Electron Microscopy. *Nano Lett.* **21**, 151–157 (2021).
15. Lewis, J. A., Tippens, J., Cortes, F. J. Q. & McDowell, M. T. Chemo-Mechanical Challenges in Solid-State Batteries. *Trends Chem.* 1–14 (2019) doi:10.1016/j.trechm.2019.06.013.
16. Herbert, E. G., Tenhaeff, W. E., Dudney, N. J. & Pharr, G. M. Mechanical characterization of LiPON films using nanoindentation. *Thin Solid Films* **520**, 413–418 (2011).
17. Xu, F. *et al.* Complete elastic characterization of lithium phosphorous oxynitride films using picosecond ultrasonics. *Thin Solid Films* **548**, 366–370 (2013).
18. Kozen, A. C., Pearse, A. J., Lin, C. F., Noked, M. & Rubloff, G. W. Atomic Layer Deposition of the Solid Electrolyte LiPON. *Chem. Mater.* **27**, 5324–5331 (2015).
19. Muñoz, F. *et al.* Increased electrical conductivity of LiPON glasses produced by

- ammonolysis. *Solid State Ionics* **179**, 574–579 (2008).
20. Westover, A. S. *et al.* Plasma Synthesis of Spherical Crystalline and Amorphous Electrolyte Nanopowders for Solid-State Batteries. *ACS Appl. Mater. Interfaces* **12**, 11570–11578 (2020).
 21. López-Aranguren, P. *et al.* Crystalline LiPON as a Bulk-Type Solid Electrolyte. *ACS Energy Lett.* 445–450 (2021) doi:10.1021/acsenerylett.0c02336.
 22. Schwöbel, A., Hausbrand, R. & Jaegermann, W. Interface reactions between LiPON and lithium studied by in-situ X-ray photoemission. *Solid State Ionics* **273**, 51–54 (2015).
 23. Le Van-Jodin, L., Ducroquet, F., Sabary, F. & Chevalier, I. Dielectric properties, conductivity and Li⁺ ion motion in LiPON thin films. *Solid State Ionics* **253**, 151–156 (2013).
 24. M. F. Vieira, E. *et al.* Flexible solid-state Ge – LiCoO₂ battery: From materials to device application. *Adv. Mater. Lett.* **8**, 820–829 (2017).
 25. Sepúlveda, A., Criscuolo, F., Put, B. & Vereecken, P. M. Effect of high temperature LiPON electrolyte in all solid state batteries. *Solid State Ionics* **337**, 24–32 (2019).
 26. Lee, J. Z. *et al.* Cryogenic Focused Ion Beam Characterization of Lithium Metal Anodes. *ACS Energy Lett.* **4**, 489–493 (2019).
 27. Hobold, G. M. *et al.* Moving beyond 99.9% Coulombic efficiency for lithium anodes in liquid electrolytes. *Nat. Energy* **6**, 951–960 (2021).
 28. Fang, C. *et al.* Pressure-tailored lithium deposition and dissolution in lithium metal batteries. *Nat. Energy* **6**, 987–994 (2021).
 29. Wang, M. J., Carmona, E., Gupta, A., Albertus, P. & Sakamoto, J. Enabling “lithium-free” manufacturing of pure lithium metal solid-state batteries through in situ plating. *Nat. Commun.* **11**, 1–9 (2020).
 30. Lee, Y. G. *et al.* High-energy long-cycling all-solid-state lithium metal batteries enabled by silver–carbon composite anodes. *Nat. Energy* **5**, 299–308 (2020).
 31. Motoyama, M., Ejiri, M. & Iriyama, Y. Modeling the Nucleation and Growth of Li at Metal Current Collector/LiPON Interfaces. *J. Electrochem. Soc.* **162**, A7067–A7071 (2015).
 32. Yan, K. *et al.* Selective deposition and stable encapsulation of lithium through heterogeneous seeded growth. *Nat. Energy* **1**, 16010 (2016).